Journal of Materials Chemistry A

ROYAL SOCIETY OF CHEMISTRY

PAPER

View Article Online
View Journal | View Issue

Check for updates

Cite this: J. Mater. Chem. A, 2024, 12, 2924

Self-assembly of Pt(II)-tetrakis(pentafluorophenyl) porphyrin *via* F···F interaction for efficient cocatalyst-free photocatalytic hydrogen evolution†

Govardhana Babu Bodedla, *[abc] Venkatesh Piradi,[c] Waygen Thor, [c] Ka-Leung Wong, [c] Xunjin Zhu *[c] and Wai-Yeung Wong *[ab]

The aggregation caused quenching (ACQ) of photoluminescence in porphyrins, which is attributed to strong π–π (C···C/C···H) interactions in the solid state, often leads to a decrease in photoluminescence, short electron lifetimes (τ_{PL}) and inferior performance in photocatalytic hydrogen evolution (PHE). To address this issue, we explore self-assembled Pt(II)-tetrakis(pentafluorophenyl)porphyrin (SA-PtPFTPP) and Pt(II)-tetraphenylporphyrin (SA-PtTPP) as candidates. We find that SA-PtPFTPP *via* F···F interaction effectively restricts ACQ in the solid state, whereas SA-PtTPP shows noticeable ACQ due to intermolecular π–π (C···C/C···H) interactions. Compared with SA-PtTPP, SA-PtPFTPP demonstrates a longer τ_{PL} value and higher photoluminescence quantum yield. Moreover, SA-PtPFTPP exhibits more efficient charge separation and better dispersibility in water with a low water contact angle. The favorable photophysical properties of SA-PtPFTPP enable a direct electron transfer from the photoexcited porphyrin moiety to the proton in cocatalyst-free PHE. As a result, SA-PtPFTPP shows a much higher PHE rate (η_{H_2}) of 400.0 μmol g^{-1} h^{-1} compared to SA-PtTPP (5.0 μmol g^{-1} h^{-1}) under heterogeneous conditions. Importantly, SA-PtPFTPP also demonstrates high photostability under prolonged irradiation, as evidenced by the consistent η_{H_2} production in each photocycle and unchanged morphology before and after light irradiation. This research provides a valuable insight into the design of self-assembled porphyrins with hindered ACQ, offering potential applications in cocatalyst-free PHE.

Received 5th September 2023
Accepted 8th December 2023

DOI: 10.1039/d3ta05389j

rsc.li/materials-a

Introduction

Self-assembled (SA) porphyrins have attracted great interest from the scientific community owing to their broad absorption in the UV-visible region, stable redox potentials, and well-defined morphology.[1–6] Nevertheless, they have been employed in many applications such as photocatalytic hydrogen evolution (PHE),[1,7,8] photodynamic therapy,[9,10] photocatalytic pollutant degradation,[11–14] optoelectronics[15,16] and biological applications.[17,18] PHE is a sustainable green technology to convert water (H_2O) into hydrogen (H_2) through artificial photosynthesis.[19–27] To date, a number of SA porphyrins have been studied for PHE and their performances mainly depend on the morphology and the capability of photoinduced charge separation and migration of charge carriers.[4] However, while SA porphyrins possess good light-harvesting properties in the solid state compared to their dilute solutions, they might suffer from aggregation caused quenching (ACQ) of photoluminescence due to the strong intermolecular π–π (C···C/C···H) interactions of porphyrin molecules in the solid state.[17] The effective inhibition of ACQ of SA porphyrins can populate the photoexcited states with longer τ_{PL}, which is beneficial in enhancing PHE through electron transfer from the photoexcited SA porphyrins to the proton (H^+). While ACQ-restricted SA porphyrins have been applied for biological studies, their application in PHE has not been reported to date.[28]

Meanwhile, previous reports on PHE mainly focused on short-lived singlet photoexcited SA Zn(II)-porphyrins.[4] But long-lived triplet photoexcited SA Pt(II)-porphyrins have been less studied for PHE. Pt(II)-porphyrins, known for the heavy atom effect of Pt, possess long-lived photoexcited triplet states due to efficient intersystem crossing (ISC).[20] These Pt(II)-porphyrins have been widely applied for biology,[29–31] water oxidation,[32]

[a]Department of Applied Biology & Chemical Technology, Research Institute for Smart Energy, The Hong Kong Polytechnic University, Hong Kong, P. R. China. E-mail: govardhan.bodedla@gmail.com; govardhana.bodedla@polyu.edu.hk; wai-yeung.wong@polyu.edu.hk

[b]The Hong Kong Polytechnic University Shenzhen Research Institute, Shenzhen 518057, P. R. China

[c]Department of Chemistry, Institute of Advanced Materials, Hong Kong Baptist University, Waterloo Road, Kowloon Tong, Hong Kong, P. R. China. E-mail: xjzhu@hkbu.edu.hk

† Electronic supplementary information (ESI) available: Materials and methods, synthesis, emission spectra, photocatalytic systems under different conditions, NMR spectra, and MALDI-TOF spectra. See DOI: https://doi.org/10.1039/d3ta05389j

optoelectronics,[33–35] sensing applications,[36–39] and self-assembly studies.[40] On the other hand, the SA *meso*-tetrakis(pentafluorophenyl)porphyrin is dominated by edge-to-face packing *via* strong fluorine–fluorine (F···F) interactions instead of intermolecular π–π stacking *via* carbon–carbon (C···C)/carbon–hydrogen (C···H) interactions in the solid state. In contrast, *meso*-tetraphenylporphyrin without F atoms forms face-to-face aggregates because of strong π–π (C···C/C···H) interactions.[41–44] As a result, Pt(II)-tetrakis(pentafluorophenyl)-porphyrin (PtTPFPP) in the solid state can avoid ACQ unlike Pt(II)-tetraphenylporphyrin (PtTPP), enabling efficient electron transfer from the photoexcited porphyrin moiety to H^+ for PHE. Therefore, studying the optoelectronic, morphological and PHE properties of the simple SA-PtPFTPP and SA-PtTPP (Fig. 1) can provide valuable insights into improving the PHE of SA porphyrins by suppressing ACQ. Our recent exploration of Pt(II)-porphyrins with long-lived photoexcited triplet states for efficient PHE supports the hypothesis that porphyrins possessing long-lived photoexcited triplet states together with suppressed ACQ in the solid state are more favorable for efficient heterogeneous PHE.[20]

Results and discussion

The synthesis of PtPFTPP and PtTPP is shown in Schemes S1 and S2.† Both porphyrins were well characterized by NMR and MALDI-TOF, and they are well soluble in dichloromethane (DCM), chloroform ($CHCl_3$), and tetrahydrofuran (THF) solvents.

Preparation of SA porphyrins

Porphyrin (2.3 mg of PtPFTPP, 1.6 mg of PtTPP, or 2.0 mg of PFTPPNH2) was dissolved in 2 mL THF and then its THF solution (100 μL) was injected into 20 mL of deionized H_2O under sonication for 5 min. Afterwards, the purple H_2O solution containing SA porphyrin was obtained by removing the THF through air flushing for 15 min at room temperature. This solution was directly used for photophysical, electrochemical, morphological, photocurrent–time, and PHE studies.

Photophysical and electrochemical studies

Fig. 2(a) shows the absorption spectra of Pt(II)-porphyrins in THF solution and SA Pt(II)-porphyrins in H_2O, and the corresponding data are given in Table 1. Pt(II)-porphyrins show two types of absorption peaks. The higher energy peaks (*ca.* 389 to 410 nm) with strong absorbance represent the Soret-band of the porphyrin ring. The lower energy peaks (*ca.* 506 to 595 nm) with weak absorbance correspond to the Q-bands of the porphyrin ring. On the other hand, SA Pt(II)-porphyrins in H_2O exhibit similar two types of peaks to Pt(II)-porphyrins in THF, but with a broader and extended absorption profile from 250 to 1000 nm. This indicates the formation of SA Pt(II)-porphyrins in the H_2O solution.[7] Notably, the Soret-band of SA-PtPFTPP in H_2O is slightly red-shifted compared to its THF solution, while SA-PtTPP in H_2O shows two split Soret-band peaks with much red-shift in comparison to its THF solution. These results suggest that the way of self-assembling in F-containing PtPFTPP is different from that of PtTPP without F. The single crystal X-ray structure of PtPFTPP has undoubtedly demonstrated that there are strong intermolecular F···F interactions between neighbouring porphyrin molecules but no π–π (C···C/C···H) interactions (Fig. 4(a)). In contrast, strong intermolecular π–π (C···C/C···H) interactions of neighbouring porphyrin molecules were observed in the single crystal X-ray structure of PtTPP (Fig. 4(b)). All these results definitely suggest that SA-PtPFTPP is mainly dominated by the edge-to-face packing *via* F···F interactions of the neighbouring porphyrin molecules in the solid state, while SA-PtTPP is provoked by the face-to-face stacking through intermolecular π–π (C···C/C···H) interactions of neighbouring porphyrin molecules.

As shown in Fig. 2(b), the emission of SA-PtTPP in H_2O is significantly quenched when compared to PtTPP in THF solution, indicating ACQ due to the strong intermolecular π–π stacking of planar porphyrin units in the solid state. In contrast, the emission intensity of SA-PtPFTPP in H_2O is comparable to that of PtPFTPP in THF solution, revealing that SA-PtPFTPP suppresses ACQ through restricted π–π stacking and dominant intermolecular F···F interactions of neighbouring porphyrin molecules in the solid state. This advantageous behaviour of SA-PtPFTPP leads to long-lived photoexcited triplet states with a longer τ_{PL}. As shown in Fig. S1(a)† and Table 1, the τ_{PL} value of SA-PtTPP (0.16 μs) in H_2O is shorter than that of PtTPP (1.70 μs) in THF solution, while the τ_{PL} value of SA-PtPFTPP (1.73 μs) in H_2O is comparable to that of PtPFTPP (1.81 μs) in THF solution. Since the photoluminescence quantum yield (Φ_{PL}) is affected by oxygen quenching, we recorded it under an argon atmosphere. The Φ_{PL} of SA-PtTPP (4%) in H_2O is lower than that of PtTPP (15%) in THF solution, while the Φ_{PL} value of SA-PtPFTPP (19%) in H_2O is the same as that of PtPFTPP (19%) in THF solution, consistent with their τ_{PL} values. Furthermore, the τ_{PL} values of SA-PtPFTPP and SA-PtTPP are on the μs scale indicating their phosphorescence nature.[19] This was also supported by the emission spectra of SA Pt(II)-porphyrins in the presence and absence of air, where the emission intensity of both SA-PtPFTPP and SA-PtTPP decreased immensely in the presence of air *versus* absence (Fig. S2(a)†). The same trend was observed for Pt(II)-porphyrins in THF solution (Fig. S2(b)†), further indicating their phosphorescence nature. Appealingly, the τ_{PL} value of SA-PtPFTPP is 11-fold longer than that of SA-PtTPP signifying that the former can produce higher PHE than the latter (*vide infra*).

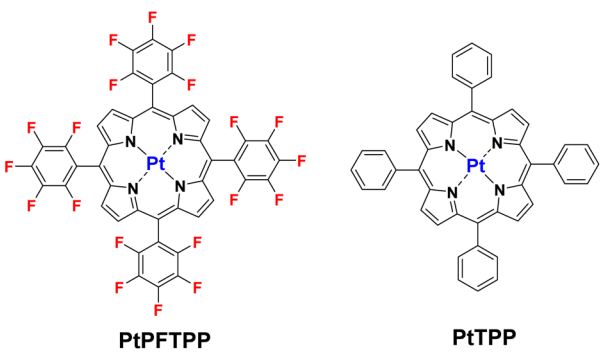

Fig. 1 Structures of the Pt(II)-porphyrins used in this study.

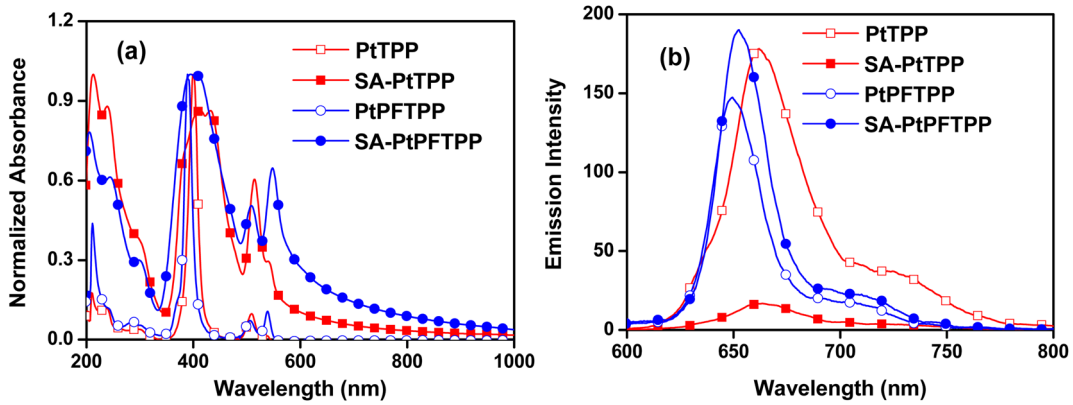

Fig. 2 (a) Absorption and (b) emission spectra of Pt(II)-porphyrins recorded in THF (10 μM) and SA Pt(II)-porphyrins recorded in H_2O at room temperature under argon.

Table 1 Photophysical and electrochemical data of the Pt(II)-porphyrins

Porphyrin	λ_{abs}[a] (nm)	λ_{abs}[b] (nm)	λ_{em}[a] (nm)	λ_{em}[b] (nm)	λ_{em}[c] (nm)	λ_{em}[d] (nm)	τ_{PL}[a] (μs)	τ_{PL}[b] (μs)	Φ_{PL}[e]	Φ_{PL}[e]	E_{VB}[f] (eV)	E_{CB}[g] (eV)	E_{0-0}[h] (eV)
PtTPP	401, 512, 542	410, 432, 515, 542	662	661	653	656	1.70	0.16	0.15	0.04	1.24	−0.93	2.17
PtPFTPP	391, 507, 541	395, 508, 549	647	649	640	641	1.81	1.73	0.21	0.19	1.40	−0.80	2.20

[a] In THF (10 μM) at room temperature under an argon atmosphere. [b] In H_2O at room temperature under an argon atmosphere. [c] In THF (10 μM) at 77 K. [d] In H_2O at 77 K. [e] $[Ru(bpy)_3]Cl_2$ in degassed acetonitrile used as a reference (λ_{exc} = 436 nm with Φ_{PL} = 0.042). [f] $E_{VB} = E_{CB} + E_{0-0}$. [g] Calculated from Mott–Schottky plots. [h] Calculated from Tauc plots.

The energy levels of the conduction band (E_{CB}) and the bandgap (E_{0-0}) of SA Pt(II)-porphyrins were calculated from Mott–Schottky (Fig. 3(a)) and Tauc plots (Fig. S3†), respectively. The valence band (E_{VB}) energy levels were derived *via* $E_{VB} = E_{CB} - E_{0-0}$. As a result, the E_{CB}/E_{VB} values were calculated to be −0.93/1.24 for SA-PtTPP and −0.80 eV/1.40 eV for SA-PtPFTPP. As depicted in Fig. 3(b), the E_{VB} energy levels of both porphyrins are lower than the TEA redox potential and E_{CB} energy levels are higher than the standard redox potential of H^+ reduction. This implies that the two SA Pt(II)-porphyrins possess favorable thermodynamic driving force for electron transfer from TEA to SA Pt(II)-porphyrins and efficient electron transfer from SA Pt(II)-porphyrins to H^+ ions during the PHE process.

Morphological studies

We further recorded the SEM images of SA Pt(II)-porphyrins, which were drop-cast on a silica substrate from their H_2O solutions. As shown in Fig. 4, SA-PtPFTPP exhibits a hexagonal microflowered structure, while SA-PtTPP shows a tetragonal microflowered structure. This signifies that the self-assembly modes of the two porphyrins are different in the solid state, which aligns with their respective photophysical properties. Additionally, powder X-ray diffraction (PXRD) analysis reveals that both Pt(II)-porphyrins exhibit highly crystalline structures, as evidenced by the sharp Bragg peaks that are almost the same as their single-crystal X-ray diffraction peaks (Fig. S4†). All these results indicate that the molecular interactions of Pt(II)-porphyrins discussed above are consistent with the experimental observations.

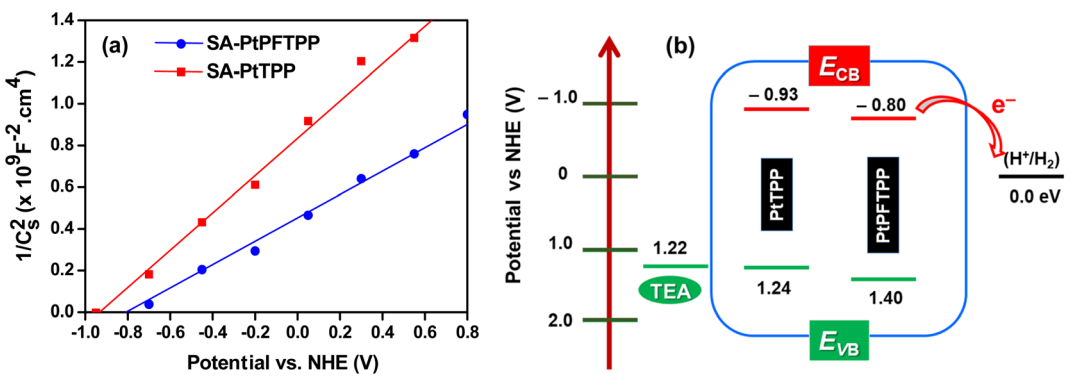

Fig. 3 (a) Mott–Schottky plots of SA Pt(II)-porphyrins and (b) energy level alignments of the components used in the photocatalytic systems.

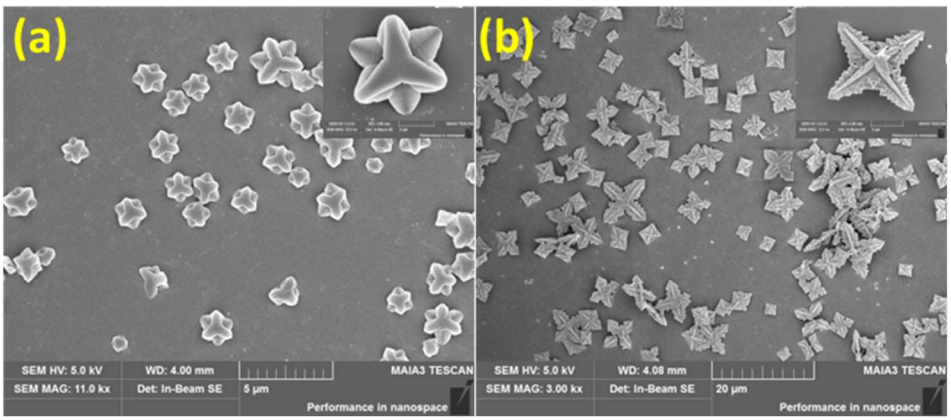

Fig. 4 (a) SEM images of (a) SA-PtPFTPP and (b) SA-PtTPP.

To get insight into the intermolecular interactions of PtPFTPP and PtTPP in the solid state, we have redrawn the crystal packing models from their single-crystal X-ray structures reported previously (Fig. 5).[42,45,46] Obviously, there are very strong F···F interactions between adjacent porphyrin PtPFTPP molecules with F···F distances within 2.863–2.900 Å, which are smaller than the van der Waals radius of the F atom (2.94 Å). Additionally, other intermolecular interactions such as C–H (pyrrole)···F interactions at 2.436 Å, C–H (pyrrole)···π (pyrrole) interactions with 2.776 Å, and F···π (benzene) interactions with 3.017 Å are observed in the PtPFTPP crystal. In contrast, PtTPP exhibits intermolecular C–H (pyrrole)···π (benzene) interactions with 2.978 Å. Additionally, intermolecular C–H (benzene)···π (pyrrole) interactions are also observed, with a H–π hydrogen bond distance of 2.716 Å. These results clearly indicate that the mode of interactions between PtPFTPP molecules in the solid state is completely different from that of PtTPP, aligning with the photophysical and morphological studies of SA-PtPFTPP and SA-PtTPP.

PHE studies

A set of heterogeneous cocatalyst-free photocatalytic systems was constructed using SA Pt(II)-porphyrins as photosensitizers

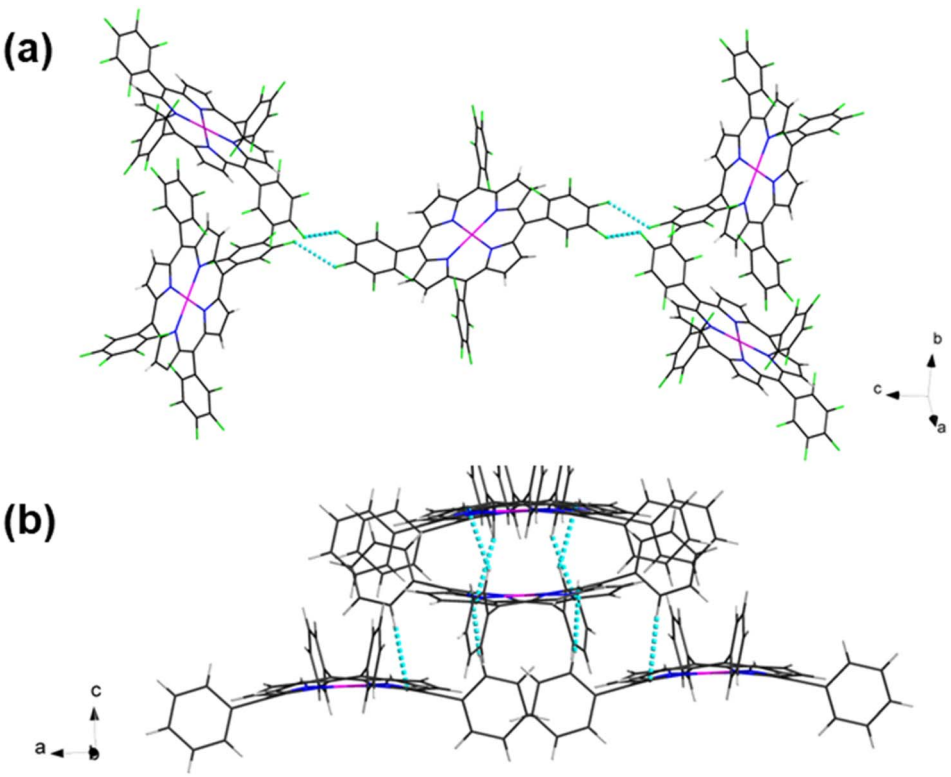

Fig. 5 Mode of interactions of (a) PtPFTPP and (b) PtTPP in their single crystals.

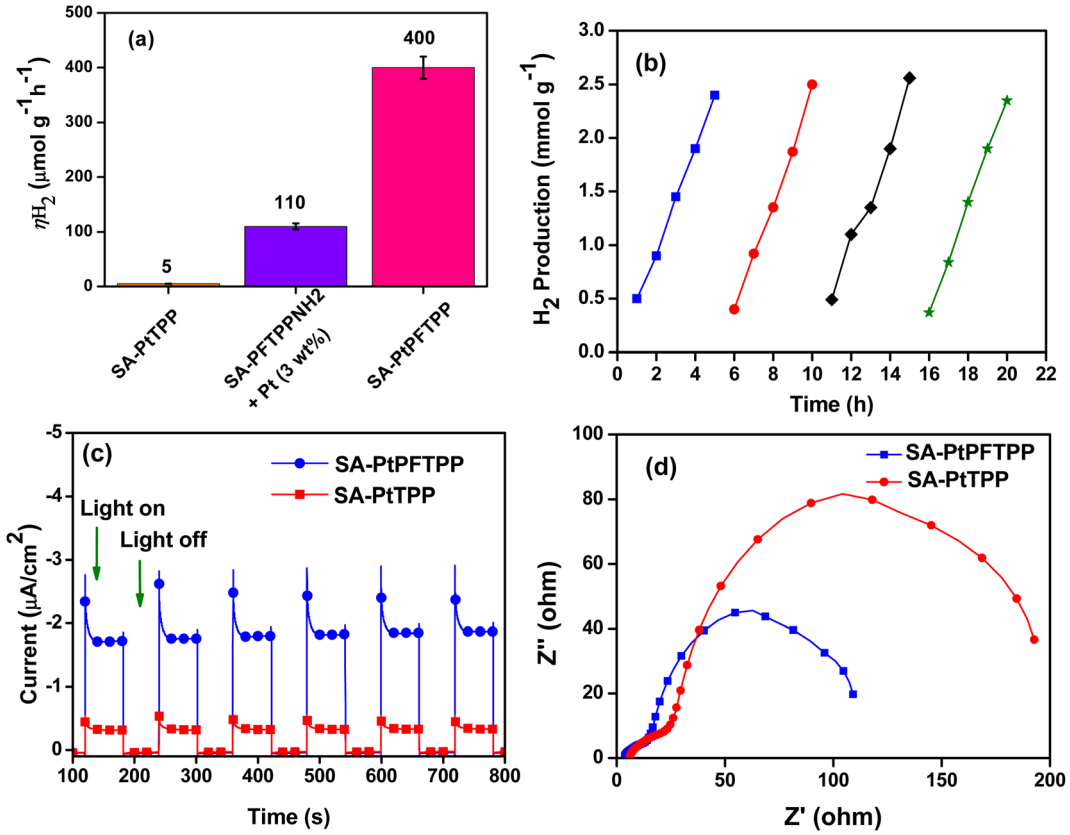

Fig. 6 (a) η_{H_2} of photocatalytic systems of SA-PtPFTPP, SA-PtTPP and SA-PFTPPNH2 under irradiation for 5 h (3 wt% Pt cocatalyst was added in the case of SA-PFTPPNH2), (b) H_2 production of different cycles of the SA-PtPFTPP photocatalytic system, (c) photocurrent–time response spectra of SA-PtPFTPP and SA-PtTPP and (d) Nyquist plots of SA-PtPFTPP and SA-PtTPP under illumination conditions.

(PSs), TEA as a sacrificial donor, and H_2O as a H^+ source. Their PHE performances are shown in Fig. 6(a). SA-PtPFTPP shows a significantly higher PHE rate (η_{H_2}) of 400.0 μmol g^{-1} h^{-1} compared to SA-PtTPP (5.0 μmol g^{-1} h^{-1}). The higher PHE performance of SA-PtPFTPP than SA-PtTPP could be attributed to the following factors: (i) long-lived photoexcited triplet states due to the restricted ACQ, (ii) efficient separation of photoinduced hole–electron pairs (*vide infra*), (iii) enhanced electron transport (*vide infra*) and (iv) better dispersibility in H_2O (*vide infra*). To further optimize the η_{H_2} of the photocatalytic systems, we examined different sacrificial donors, namely, triethanolamine (TEOA), ethylenediaminetetraacetic acid (EDTA), 1,3-dimethyl-2-phenylbenzimidazoline (BIH) and ascorbic acid (AA) (Fig. S5†). The results demonstrated that the TEA-based photocatalytic systems exhibited superior PHE performance compared to the TEOA, EDTA, BIH and AA systems. We also tested the PHE of SA Pt(II)-porphyrins without the TEA sacrificial donor, but unfortunately, no significant H_2 was detected. This indicates that TEA is needed for converting SA Pt(II)-porphyrins into potential reductants through a reductive quenching pathway (*vide infra*). Furthermore, the PHE of SA-PFTPPH2 without the Pt metal centre was investigated. The results showed that SA-PFTPPNH2 did not produce any H_2, while the presence of 3 wt% Pt cocatalyst produced a η_{H_2} of 110.0 μmol g^{-1} h^{-1}, which is even 4-fold lower than that of SA-PtPFTPP without the Pt cocatalyst. This indicates that the long-lived photoexcited triplet states of SA-PtPFTPP, along with restricted ACQ, enable the efficient transfer of electrons from the photoexcited triplet states of the porphyrin moiety to H^+ for H_2O reduction.

To assess the photostability of SA-PtPFTPP, we conducted four consecutive PHE experiments over 20 h of light irradiation. As shown in Fig. 6(b), the photocatalytic system of SA-PtPFTPP produced similar levels of H_2 production in each photocycle and the morphology of SA-PtPFTPP did not change before and after 20 h of light irradiation (Fig. S6†), demonstrating the remarkable photostability of SA-PtPFTPP. In contrast, the photocatalytic system of SA-PtTPP did not produce consistent H_2 production (Fig. S9†) in each photocycle and the morphology of SA-PtPFTPP changed (Fig. S7†) after 20 h of light irradiation. This indicates that SA-PtTPP is not very photostable under long irradiation. Additionally, the time-dependent PHE of SA Pt(II)-porphyrins was studied by monitoring the PHE of photocatalytic systems over 20 h of light irradiation from the initial time. As shown in Fig. S8(a),† the PHE of SA-PtPFTPP is continuously increased from the initial time of light irradiation to 20 h, while the PHE of SA-PtTPP reached a plateau after 10 h of light irradiation (Fig. S8(b)†). This result aligns well with the findings above. These results indicate that the higher photostability of SA-PtPFTPP might be attributed to the stronger

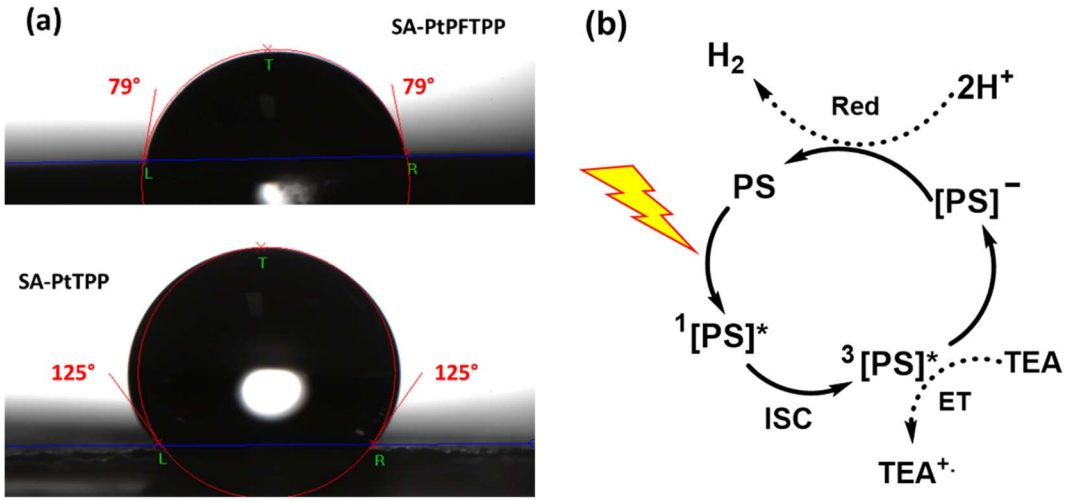

Fig. 7 H_2O contact angle measurements of (a) SA-PtPFTPP and SA-PtTPP in H_2O and (b) proposed cyclic PHE mechanism of SA Pt(II)-porphyrins (PS = SA Pt(II)-porphyrins, ET = electron transfer and Red = reduction).

intermolecular F···F interactions in the solid state when compared to SA-PtTPP with intermolecular π–π (C···C/C···H) interactions.

To understand the separation of photogenerated hole–electron pairs, we recorded the transient photocurrent–time response spectra (*i*–*t* curves) of SA Pt(II)-porphyrins drop-cast on an ITO plate from their H_2O solutions.[1,47] As shown in Fig. 6(c), SA-PtPFTPP shows a higher photocurrent response than SA-PtTPP, illustrating more efficient separation of photogenerated hole–electron pairs for SA-PtPFTPP. Moreover, the electron transport resistance (R_{ct2}) of SA Pt(II)-porphyrins was studied using the Nyquist plot to assess electron migration. As shown in Fig. 6(d), the radius of the middle large semicircle in the Nyquist plot corresponds to R_{ct2}. Notably, SA-PtPFTPP exhibits a lower R_{ct2} than SA-PtTPP, indicating an enhanced electron migration within SA-PtPFTPP under illumination conditions. These findings also well match to the higher PHE of SA-PtPFTPP than SA-PtTPP when employing PSs in the PHE systems.

Because the dispersibility of PSs in H_2O also affects the PHE of heterogeneous PHE systems, we performed the contact angle measurements of SA Pt(II)-porphyrins in H_2O.[48,49] As shown in Fig. 7(a), the contact angle of SA-PtPFTPP is 79°, which is much lower than that of SA-PtTPP (125°). This indicates that SA-PtPFTPP possesses less hydrophobic nature, resulting in better dispersibility in H_2O compared to SA-PtTPP. This improved dispersibility could be attributed to the F atoms in SA-PtPFTPP, which form hydrogen bonds with H_2O.[50] As a result, the reaction collision possibility is elevated, leading to enhanced PHE activity of SA-PtPFTPP compared to SA-PtTPP.

To investigate whether the PHE process follows a reductive quenching mechanism, we performed the photoluminescence quenching studies of SA Pt(II)-porphyrins in the presence of a TEA quencher. As seen in Fig. S10,† the emission intensity of SA Pt(II)-porphyrins gradually decreases with increasing TEA concentration, indicating efficient electron transfer from TEA to photoexcited SA Pt(II)-porphyrins under light illumination. This also explains that the photocatalytic systems of SA Pt(II)-porphyrins did not produce any H_2 in the absence of a TEA sacrificial donor. Based on the aforementioned studies and results, we presented a schematic illustration of the PHE of SA Pt(II)-porphyrins as shown in Fig. 7(b). Upon light irradiation on the SA Pt(II)-porphyrins (PS), the first step involves photoexcitation, resulting in photoexcited singlet states. Subsequently, in the second step, the photoexcited singlet states are converted to photoexcited triplet states *via* an ISC process. At this stage, the reductant PS is formed by acquiring electrons from TEA, which later transfer electrons to H^+ for H_2 production.

Conclusions

In summary, we conducted a comprehensive study on the photophysical, electrochemical, morphological, and PHE properties of SA-PtPFTPP and the control SA-PtTPP. Our findings reveal distinct self-assembly modes for PtPFTPP and PtTPP in the solid state, primarily due to F···F interactions in SA-PtPFTPP and π–π (C···C/C···H) interactions in SA-PtTPP. The self-assembly of Pt(II)-porphyrins in H_2O solution was confirmed by a broader absorption profile compared to their dilute THF solutions. The π–π (C···C/C···H) interactions in SA-PtTPP promoted ACQ and thus gave shorter τ_{PL} values and lower Φ_{PL}, whilst the dominant F···F interactions in SA-PtPFTPP effectively restricted ACQ and consequently led to long-lived photoexcited triplet states with longer τ_{PL} values and higher Φ_{PL}. The different intermolecular interactions of SA Pt(II)-porphyrins were directly reflected in their morphology in the solid state, with hexagonal and tetragonal micro-flowered structures observed for SA-PtPFTPP and SA-PtTPP, respectively. Additionally, SA-PtPFTPP exhibited a higher photocurrent–time response, indicating more efficient separation and migration of photogenerated hole–electron pairs. H_2O contact angle measurement illustrated that SA-PtPFTPP had a lower

H_2O contact angle, indicating its better dispersibility in H_2O. As a result of the long-lived photoexcited triplet states, efficient photoinduced charge separation and better dispersibility in H_2O, enhanced electron transfer from photoexcited SA-PtPFTPP to H^+ occurred, and thereby gave a cocatalyst-free PHE rate (η_{H_2}) of 400.0 μmol g^{-1} h^{-1} which is 80-fold higher than that of SA-PtTPP ($\eta_{H_2} = 5.0$ μmol g^{-1} h^{-1}).

Author contributions

G. B. Bodedla synthesized and characterized two porphyrins used in this manuscript and performed the experiments such as UV-Vis, photoluminescence, and PHE experiments, and wrote the original manuscript. V. Piradi performed SEM studies and analyzed the data. W. Thor performed phosphorescence experiments. K.-L. Wong supervised the phosphorescence studies. W.-Y. Wong and X. Zhu supervised the research project and revised the manuscript. All the authors discussed the results and evaluated the manuscript.

Conflicts of interest

There are no conflicts to declare.

Acknowledgements

G. B. B acknowledges the financial support from the Start-up Fund for RAPs under the Strategic Hiring Scheme (P0048725) of the Hong Kong Polytechnic University. W.-Y. W. acknowledges the financial support from the RGC Senior Research Fellowship Scheme (SRFS2021-5S01), the National Natural Science Foundation of China (52073242), the Hong Kong Polytechnic University (YXA2), the Research Institute for Smart Energy (CDAQ) and Ms Clarea Au for the Endowed Professorship in Energy (847S). X. Z. acknowledges the funding from the General Research Fund (HKBU 12304320) and NSFC/RGC Joint Research Scheme (N_HKBU213/22), and Initiation Grant for Faculty Niche Research Areas (IG-FNRA) (2020/21)-RC-FNRA-IG/20-21/SCI/06 from Hong Kong Baptist University.

Notes and references

1 G. B. Bodedla, J. Huang, W.-Y. Wong and X. Zhu, *ACS Appl. Nano Mater.*, 2020, **3**, 7040–7046.
2 Y. Ji, Q. Zuo, C. Chen, Y. Liu, Y. Mai and Y. Zhou, *Chem. Commun.*, 2021, **57**, 4174–4177.
3 T. E. Karam, N. Siraj, J. C. Ranasinghe, P. E. Kolic, B. P. Regmi, I. M. Warner and L. H. Haber, *J. Phys. Chem. C*, 2020, **124**, 24533–24541.
4 Y. Zhong, S. Liu, J. Wang, W. Zhang, T. Tian, J. Sun and F. Bai, *APL Mater.*, 2020, **8**, 120706.
5 G. Magna, D. Monti, C. Di Natale, R. Paolesse and M. Stefanelli, *Molecules*, 2019, **24**, 4307.
6 J. Tian and W. Zhang, *Prog. Polym. Sci.*, 2019, **95**, 65–117.
7 Y. Zhong, Y. Hu, J. Wang, J. Wang, X. Ren, J. Sun and F. Bai, *MRS Adv.*, 2019, **4**, 2071–2078.
8 B. Cai, H. Song, A. Brnovic, M. V. Pavliuk, L. Hammarström and H. Tian, *J. Am. Chem. Soc.*, 2023, **145**, 18687–18692.
9 J. Li, W. Sun, Z. Yang, G. Gao, H.-H. Ran, K.-F. Xu, Q.-Y. Duan, X. Liu and F.-G. Wu, *ACS Appl. Mater. Interfaces*, 2020, **12**, 54378–54386.
10 Q. Wang, Q. Chen, G. Jiang, M. Xia, M. Wang, Y. Li, X. Ma, J. Wang and X. Gu, *Chin. Chem. Lett.*, 2019, **30**, 1965–1968.
11 D. Zhang, X. Huang, J. Huang, Y. Li and J. Cai, *J. Porphyrins Phthalocyanines*, 2021, **25**, 298–306.
12 Y. Chen, A. Li, Z.-H. Huang, L.-N. Wang and F. Kang, *Nanomaterials*, 2016, **6**, 51.
13 N. K. Shee and H.-J. Kim, *Molecules*, 2021, **26**, 3598.
14 D. D. La, T. A. Nguyen, X. S. Nguyen, T. N. Truong, H. P. Nguyen T, H. D. Ninh, H. T. Vo, S. V. Bhosale, S. W. Chang, E. R. Rene, T. H. Nguyen, S. M. Lee, L. D. Tran and D. D. Nguyen, *J. Environ. Chem. Eng.*, 2021, **9**, 106034.
15 Z. Tao, R. Li, X. Xu, A. Cao, W. You, Y. He, W. Huang, L. Kang and X. Chen, *Cryst. Growth Des.*, 2021, **21**, 3582–3591.
16 G. B. Bodedla, X. Zhu, Z. Zhou and W.-Y. Wong, *Top. Curr. Chem.*, 2022, **380**, 49.
17 G. B. Bodedla, X. Zhu and W.-Y. Wong, *Aggregate*, 2023, **4**, e330.
18 X. Wang, J. Wang, J. Wang, Y. Zhong, L. Han, J. Yan, P. Duan, B. Shi and F. Bai, *Nano Lett.*, 2021, **21**, 3418–3425.
19 G. B. Bodedla, D. N. Tritton, X. Chen, J. Zhao, Z. Guo, K. C.-F. Leung, W.-Y. Wong and X. Zhu, *ACS Appl. Energy Mater.*, 2021, **4**, 3945–3951.
20 G. B. Bodedla, Y. Dong, G. Tang, J. Zhao, F. Zhang, X. Zhu and W.-Y. Wong, *J. Mater. Chem. A*, 2022, **10**, 13402–13409.
21 G. B. Bodedla, V. Piradi, M. Imran, J. Zhao, X. Zhu and W.-Y. Wong, *J. Mater. Chem. A*, 2023, **11**, 1473–1481.
22 D. N. Tritton, G. B. Bodedla, G. Tang, J. Zhao, C.-S. Kwan, K. C.-F. Leung, W.-Y. Wong and X. Zhu, *J. Mater. Chem. A*, 2020, **8**, 3005–3010.
23 G. B. Bodedla, L. Li, Y. Che, Y. Jiang, J. Huang, J. Zhao and X. Zhu, *Chem. Commun.*, 2018, **54**, 11614–11617.
24 F. Zhang, J. Zhang, J. Li, X. Jin, Y. Li, M. Wu, X. Kang, T. Hu, X. Wang, W. Ren and G. Zhang, *J. Mater. Chem. A*, 2019, **7**, 6939–6945.
25 H. Wang, J. Zhang, X. Jin, X. Wang, F. Zhang, J. Xue, Y. Li, J. Li and G. Zhang, *J. Mater. Chem. A*, 2021, **9**, 7143–7149.
26 F. Zhang, J. Li, H. Wang, Y. Li, Y. Liu, Q. Qian, X. Jin, X. Wang, J. Zhang and G. Zhang, *Appl. Catal., B*, 2020, **269**, 118772.
27 K. Zheng, G. B. Bodedla, Y. Hou, J. Zhang, R. Liang, J. Zhao, D. Lee Phillips and X. Zhu, *J. Mater. Chem. A*, 2022, **10**, 4440–4445.
28 C.-C. Chang, M.-C. Hsieh, J.-C. Lin and T.-C. Chang, *Biomaterials*, 2012, **33**, 897–906.
29 V. A. Oliveira, B. A. Iglesias, B. L. Auras, A. Neves and H. Terenzi, *Dalton Trans.*, 2017, **46**, 1660–1669.
30 L. Q. Soares Lopes, A. P. Ramos, P. M. Copetti, T. V. Acunha, B. A. Iglesias, R. C. Vianna Santos, A. K. Machado and M. R. Sagrillo, *Microb. Pathog.*, 2019, **128**, 47–54.
31 A. Naik, R. Rubbiani, G. Gasser and B. Spingler, *Angew. Chem., Int. Ed.*, 2014, **53**, 6938–6941.

32 H.-C. Chen, D. G. H. Hetterscheid, R. M. Williams, J. I. van der Vlugt, J. N. H. Reek and A. M. Brouwer, *Energy Environ. Sci.*, 2015, **8**, 975–982.
33 K. R. Graham, Y. Yang, J. R. Sommer, A. H. Shelton, K. S. Schanze, J. Xue and J. R. Reynolds, *Chem. Mater.*, 2011, **23**, 5305–5312.
34 L. Huang, C. D. Park, T. Fleetham and J. Li, *Appl. Phys. Lett.*, 2016, **109**, 233302.
35 Y. Gao, V. Piradi, X. Zhu and S. K. So, *ACS Appl. Energy Mater.*, 2022, **5**, 4916–4925.
36 H. Xiang, L. Zhou, Y. Feng, J. Cheng, D. Wu and X. Zhou, *Inorg. Chem.*, 2012, **51**, 5208–5212.
37 E. Fagadar-Cosma, N. Plesu, A. Lascu, D. Anghel, M. Cazacu, C. Ianasi, G. Fagadar-Cosma, I. Fratilescu and C. Epuran, *Chemosensors*, 2020, **8**, 29.
38 Y. Mao, Q. Zhao, T. Pan, J. Shi, S. Jiang, M. Chen, B. Zhou and Y. Tian, *New J. Chem.*, 2017, **41**, 5429–5435.
39 G. Pandey, R. Chaudhari, B. Joshi, S. Choudhary, J. Kaur and A. Joshi, *Sci. Rep.*, 2019, **9**, 5029.
40 X.-D. Xu, J. Zhang, L.-J. Chen, R. Guo, D.-X. Wang and H.-B. Yang, *Chem. Commun.*, 2012, **48**, 11223–11225.
41 S. K. Das, B. Song, A. Mahler, V. N. Nesterov, A. K. Wilson, O. Ito and F. D'Souza, *J. Phys. Chem. C*, 2014, **118**, 3994–4006.
42 A. Hazell, *Acta Crystallogr., Sect. C: Cryst. Struct. Commun.*, 1984, **40**, 751–753.
43 P. Dechan, G. D. Bajju and P. Sood, *Crystallogr. Rep.*, 2020, **65**, 933–946.
44 S.-W. Lai, Y.-J. Hou, C.-M. Che, H.-L. Pang, K.-Y. Wong, C. K. Chang and N. Zhu, *Inorg. Chem.*, 2004, **43**, 3724–3732.
45 K. Lau, M. Gouterman, G. Khalil, M. Sadilek, E. Shankland, B. Zelow and W. Kaminsky, CCDC 252891.
46 A. Hazell, CCDC 1124153.
47 G. B. Bodedla, M. Imran, J. Zhao, X. Zhu and W.-Y. Wong, *Aggregate*, 2023, **4**, e364.
48 C.-L. Chang, W.-C. Lin, L.-Y. Ting, C.-H. Shih, S.-Y. Chen, T.-F. Huang, H. Tateno, J. Jayakumar, W.-Y. Jao, C.-W. Tai, C.-Y. Chu, C.-W. Chen, C.-H. Yu, Y.-J. Lu, C.-C. Hu, A. M. Elewa, T. Mochizuki and H.-H. Chou, *Nat. Commun.*, 2022, **13**, 5460.
49 Q. Zuo, K. Feng, J. Zhong, Y. Mai and Y. Zhou, *CCS Chem.*, 2021, **3**, 1963–1971.
50 R. E. Rosenberg, *J. Phys. Chem. A*, 2012, **116**(44), 10842–10849.